Eur. Phys. J. C 8, 679–688 (1999)
DOI 10.1007/s100529900003

THE EUROPEAN
PHYSICAL JOURNAL C


# The low energy limit of the minimal nonlinear supersymmetric SU(5)-model; production and decay of Higgs particles

H. Franz, B.R. Kim, M. Weber

III. Physikalisches Institut A, RWTH Aachen, D-52056 Aachen, Germany

Recieved: 28 October 1998 / Revised version: 17 December 1998 / Published online: 1 March 1999

**Abstract.** We consider the Higgssector in the low energy limit of the minimal nonlinear supersymmetric SU(5) model. We estimate radiative corrections to the Higgs masses using the effective potential. Furthermore Higgs boson decays are investigated and differences to the MSSM are discussed.

## 1 Introduction

Supersymmetric models have been with us for more than twenty years. Almost all of these models are linear supersymmetric models, i.e. supersymmetry (SUSY) is realized linearly. Linear SUSY models require a SUSY partner to every conventional particle. Search for SUSY particles is one of the main goals of the present and future collider experiments. So far no SUSY partners have been found. However SUSY may well be realized nonlinearly [1]. A characteristic property of the nonlinear realization is that no SUSY partners are required. In global nonlinear SUSY models the only additional field that has to be introduced is the Akulov-Volkov field (A-V field), a goldstino. But in experiment no goldstino has been observed [2]. A possibility to avoid the massless physical goldstino is to go to curved space, to supergravity. The formalism for extending the standard model in a nonlinearly supersymmetric way in curved space was developed by Samuel and Wess [3]. In supergravity the goldstino can be gauged away; the massless gravitino absorbs the goldstino and becomes massive, whereas the graviton remains massless [4]. In the limit of flat space, where the supergravity multiplet decouples from the ordinary matter, the fermion particle spectrum is the same as in the standard model. The only reminiscence of SUSY manifests itself in the Higgs sector. The Higgs sector has to be extended as in the case of linear SUSY models. Minimal nonlinear SUSY standard model [5] contains two Higgs doublets and a Higgs singlet and is a nonlinear SUSY alternative to the linear SUSY model, the Next-to-Minimal Supersymmetric Standard Model (NMSSM) [6]. It has been shown that there are typical differences in the structure of the Higgs potential between these two models. Physical consequences of this nonlinear SUSY standard model in the flat space limit were investigated, in particular, how to test the model at future $e^+e^-$-colliders [7,8]. In the meantime we also constructed a minimal nonlinear SUSY SU(5) model [9]. It turned out that the Higgs sector of this model at low energies is determined by two Higgs doublets, resembling that of the linear minimal SUSY standard model (MSSM). In a recent article [10] we derived the low energy tree level Higgs potential of this nonlinear SUSY SU(5) model, mass eigenstates and mass relations and compared them to those of the MSSM and discussed how to distinguish between the two models. We also investigated Higgs particle production at $e^+e^-$ linear colliders. In this note we consider contributions of radiative corrections using one-loop effective potential to the processes discussed in the earlier paper [10]. Further we investigate decays of Higgs particles and work out differences to MSSM.

## 2 The one-loop effective potential

The tree level Higgs potential in the low energy limit was derived in [10] and reads as follows

$$\begin{aligned} V = & \frac{1}{8}(g_1^2+g_2^2)\left(|H_1|^2-|H_2|^2\right)^2+\frac{1}{2}g_2^2|H_1^\dagger H_2|^2 \\ & +\lambda^2\left[|H_1|^2|H_2|^2-\frac{1}{5}|H_1^T\epsilon H_2|^2\right] \\ & +m_1^2|H_1|^2+m_2^2|H_2|^2+m_3^2(H_1^T\epsilon H_2+\text{ h.c.}), \quad (1) \end{aligned}$$

where $g_1$, $g_2$ and $g_3$ are the coupling constants of U(1), SU(2) and SU(3) respectively, $m_1$, $m_2$, $m_3$ are mass parameters of electroweak scale and $\lambda$ is a dimensionless self coupling.

We will now consider the effects of one-loop radiative corrections to the low energy theory. In this paper we only consider the contributions of the top and bottom quarks, which are the dominant contributions. The relevant interaction terms are given by the Yukawa part of the low energy Lagrange density

$$\begin{aligned} \mathcal{L}_{\text{Yuk,t}} &= h_t\bar{Q}_L\varepsilon H_2 t_R + h_t\bar{t}_R\, H_2^{\text{T}\,*}\varepsilon Q_L \\ \mathcal{L}_{\text{Yuk,b}} &= h_b\bar{Q}_L\varepsilon H_1 b_R + h_b\bar{b}_R\, H_1^{\text{T}\,*}\varepsilon Q_L \qquad (2) \end{aligned}$$

with

$$Q_L = \begin{pmatrix} t_L \\ b_L \end{pmatrix}, \quad \varepsilon = \begin{pmatrix} 0 & -1 \\ 1 & 0 \end{pmatrix}$$
$$q_L = \tfrac{1}{2}(1-\gamma^5)q, \quad q_R = \tfrac{1}{2}(1+\gamma^5)q$$
$$h_t = \tfrac{m_t}{\sqrt{2}v_2}, \quad h_b = \tfrac{m_b}{\sqrt{2}v_1} \tag{3}$$

We obtain the following result for the neutral part of the effective potential [11]:

$$\begin{aligned} V_{\text{eff}} &= V_0 + \Delta V_1 \\ &= \frac{1}{8}(g_1^2+g_2^2)\left(\left|H_1^0\right|^2 - \left|H_2^0\right|^2\right)^2 + \frac{4}{5}\lambda^2\left|H_1^0\right|^2\left|H_2^0\right|^2 \\ &\quad + m_1^2\left|H_1^0\right|^2 + m_2^2\left|H_2^0\right|^2 + m_3^2\left(H_1^0\, H_2^{0\,*} + \text{h.c}\right) \\ &\quad - \frac{3}{16\pi^2}h_t^4\left|H_2^0\right|^4\left\{\log\left(\frac{\left|H_2^0\right|^2}{\mu^2}\right) - \frac{3}{2}\right\} \\ &\quad - \frac{3}{16\pi^2}h_b^4\left|H_1^0\right|^4\left\{\log\left(\frac{\left|H_1^0\right|^2}{\mu^2}\right) - \frac{3}{2}\right\} \end{aligned} \tag{4}$$

with $\mu$ being the mass parameter of dimensional regularisation.

### 2.1 Mass spectra at one loop level

The extremum conditions

$$\langle \partial V_{\text{eff}}/\partial v_1 \rangle_0 = 0, \langle \partial V_{\text{eff}}/\partial v_2 \rangle_0 = 0$$

yield the relations

$$\begin{aligned} m_1^2 &= m^2\frac{v_2^2}{v^2} - \frac{1}{8}g^2\left(v_1^2 - v_2^2\right) - L_1\frac{v_1^4}{v^2} + L_2\frac{v_2^4}{v^2} \\ m_2^2 &= m^2\frac{v_1^2}{v^2} + \frac{1}{8}g^2\left(v_1^2 - v_2^2\right) + L_1\frac{v_1^4}{v^2} - L_2\frac{v_2^4}{v^2} \\ m_3^2 &= -\left(\frac{2}{5}\lambda^2 + \frac{m^2}{v^2}\right)v_1v_2 - L_1\frac{v_1^3v_2}{v^2} - L_2\frac{v_1v_2^3}{v^2} \end{aligned} \tag{5}$$

where we have abbreviated the logarithmic terms from $V_{\text{eff}}$ with

$$\begin{aligned} L_1 &= -\frac{3}{16\pi^2}h_b^4\left\{\log\frac{v_1^2}{2\mu^2} - 1\right\} \\ L_2 &= -\frac{3}{16\pi^2}h_t^4\left\{\log\frac{v_2^2}{2\mu^2} - 1\right\} \\ L_1' &= -\frac{9}{16\pi^2}h_b^4\left\{\log\frac{v_1^2}{2\mu^2} - \frac{1}{3}\right\} \\ L_2' &= -\frac{9}{16\pi^2}h_t^4\left\{\log\frac{v_2^2}{2\mu^2} - \frac{1}{3}\right\} \end{aligned} \tag{6}$$

The scalar and pseudoscalar mass matrices are given by

$$M^2_{\eta\,ij} = \left\langle \frac{\partial^2 V_{\text{eff}}}{\partial\eta_i\partial\eta_j}\right\rangle_0 \tag{7}$$

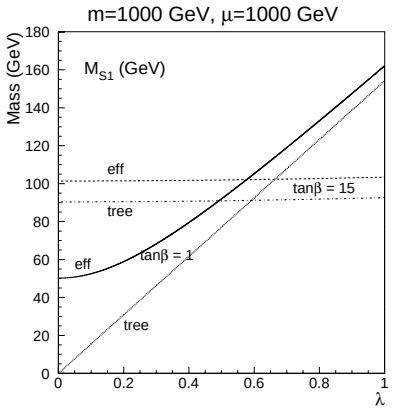


**Fig. 1.** $m_{S_1,\,\text{tree}}$ and $m_{S_1,\,\text{eff}}$ at $m = \mu = 1000$ GeV, $\tan\beta = 1(15)$, $m_t = 175\,\text{GeV}$ and $m_b = 4.3\,\text{GeV}$

$$\begin{aligned} M^2_{\eta\,11} &= \left(\frac{1}{4}g^2 - L_1\frac{v_1^2}{v^2} + L_1'\right)v_1^2 \\ &\quad + \left(\frac{2}{5}\lambda^2 + \frac{m^2}{v^2} + L_2\frac{v_2^2}{v^2}\right)v_2^2 \\ M^2_{\eta\,22} &= \left(\frac{1}{4}g^2 - L_2\frac{v_2^2}{v^2} + L_2'\right)v_2^2 \\ &\quad + \left(\frac{2}{5}\lambda^2 + \frac{m^2}{v^2} + L_1\frac{v_1^2}{v^2}\right)v_1^2 \\ M^2_{\eta\,12} &= \left(\frac{2}{5}\lambda^2 - \frac{1}{4}g^2 - \frac{m^2}{v^2} - L_1\frac{v_1^2}{v^2} - L_2\frac{v_2^2}{v^2}\right)v_1v_2 \\ &= M^2_{\eta\,12} \end{aligned}$$

$$\begin{aligned} M^2_{a\,ij} &= \left\langle \frac{\partial^2 V_{\text{eff}}}{\partial a_i\partial a_j}\right\rangle_0 \\ M^2_{a\,11} &= \left(\frac{2}{5}\lambda^2 + \frac{m^2}{v^2} + L_2\frac{v_2^2}{v^2}\right)v_2^2 + \left(L_1' - L_1\frac{v_1^2}{v^2}\right)v_1^2 \\ M^2_{a\,22} &= \left(\frac{2}{5}\lambda^2 + \frac{m^2}{v^2} + L_1\frac{v_1^2}{v^2}\right)v_1^2 + \left(L_2' - L_2\frac{v_2^2}{v^2}\right)v_2^2 \\ M^2_{a\,12} &= \left(\frac{2}{5}\lambda^2 + \frac{m^2}{v^2} + L_1\frac{v_1^2}{v^2} + L_2\frac{v_2^2}{v^2}\right)v_1v_2 \\ &= M^2_{a\,21} \end{aligned} \tag{8}$$

The mass eigenstates and mixing angles follow from these mass matrices. The expressions for the neutral scalar masses $m_{S_1,\text{eff}}$, $m_{S_2,\text{eff}}$ and the mixing angles are lengthy and we do not present them here. However the mass of the physical pseudoscalar $m_{P,\text{eff}}$ is given by the simple form

$$m_P = \frac{2}{5}\lambda^2v^2 + m^2 + L_1'v_2^2 + L_2'v_1^2 \tag{9}$$

In order to illustrate the contribution of radiative corrections we plot $m_{S_1,\text{eff}}$, $m_{S_1,\text{tree}}$ and $m_{P,\text{eff}}$ for the parameter values $m = 1000$ GeV, $\mu = 1000$ GeV, $m_t = 175$ GeV and $m_b = 4.3$ GeV in Figs. 1–2.

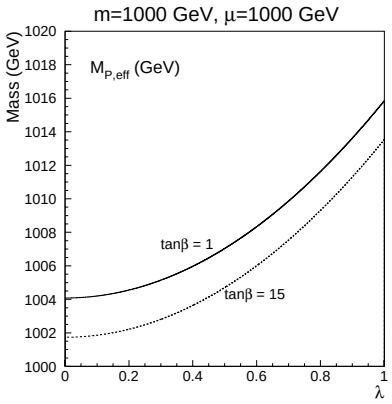


**Fig. 2.** $m_{P,\,\mathrm{eff}}$ at $m = \mu = 1000$ GeV, $\tan\beta = 1(15)$, $m_t = 175\,\mathrm{GeV}$ and $m_b = 4.3\,\mathrm{GeV}$

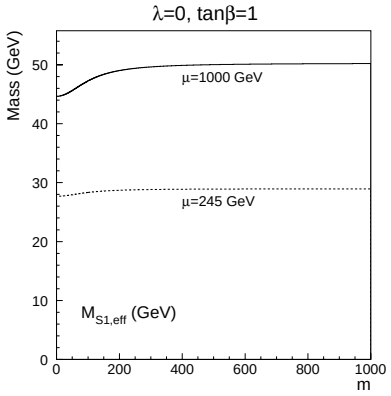


**Fig. 3.** $m_{S_1,\,\mathrm{eff}}$ for $\tan\beta = 1$, $\lambda = 0$ and $\mu = 245(1000)\,\mathrm{GeV}$

The best place, where the importance of radiative corrections manifests itself is the point $\tan\beta = 1$, $\lambda = 0$; at this point the lighter scalar mass $m_{S_1}$ vanishes at tree level

$$m_{S_1,\mathrm{tree}}(\tan\beta = 1, \lambda = 0) = 0.$$

Figure 3 shows that radiative correction generally removes this state of massless $S_1$. The pseudoscalar mass $m_P$ is independent of $\tan\beta$ at tree level, but slightly dependent on $\tan\beta$ with radiative correction as can be seem from Fig. 2.

## 3 Bounds on the lightest scalar mass

In experimental searches for Higgs particles it is very important to know theoretical upper and lower bounds for their masses.

The upper bound of $m_{S_1}$ at tree level was given in [10]. An upper bound of 0.7 on $\lambda$ can be determined through RGE analysis by demanding that $\lambda$ does not develop a Landau pole up to GUT scale [12]. Thus we obtain at tree level

$$0 \lesssim m_{S_1,\mathrm{tree}} \lesssim 110\ \mathrm{GeV}. \tag{10}$$

In order to obtain the bounds at one loop level we systematically scan the parameter space and vary $\mu$ from 245 GeV to 1000 GeV.

As can be seen from Fig. 3 the minimum occurs at $\lambda = 0$, $\tan\beta = 1$ and $\mu = 245$ GeV and is about 28 GeV. It is almost independent of m.

The maximum of $m_{S_1}$ for fixed values of $m$ and $\mu$ occurs for $\tan\beta = 1$ and maximal $\lambda$ as can be expected from Fig. 1. Figure 4 shows $m_{S_1}$ in the $\mu - m$-plane for $\tan\beta = 1$ and $\lambda = 0.7$. The absolute maximum of $m_{S_1}$ occurs at $\tan\beta = 1$, $\lambda = 0.7$, $\mu = 1000\,\mathrm{GeV}$ and $m \gtrsim 300\,\mathrm{GeV}$. Thus we obtain at one loop level

$$28\ \mathrm{GeV} \leq m_{S_1} \leq 119\ \mathrm{GeV}. \tag{11}$$

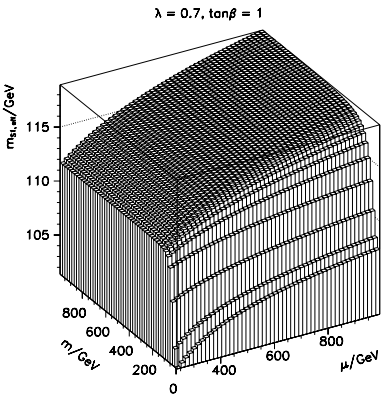


**Fig. 4.** $m_{S_1,\,\mathrm{eff}}$ for $\lambda = 0.7$ and $\tan\beta = 1$

## 4 Production of Higgs bosons at $e^+e^-$ colliders

We will now investigate the production of Higgs bosons in $e^+e^-$ reactions using the effective potential and compare the results to the tree level results we obtained in our previous article [10]. We will concentrate on the reaction

$$e^+e^- \longrightarrow Z_0^*, \gamma^* \longrightarrow S_i b\bar{b} \tag{12}$$

because the production of b quarks is dominant below the top threshold.

There are four reaction channels that contribute to the cross section:

$$\begin{aligned}
&\text{(i)}\ \ e^+e^- \to Z \to ZS_i \to \bar{f}fS_i\\
&\text{(ii)}\ \ e^+e^- \to Z \to \bar{f}f \to \bar{f}fS_i\\
&\text{(iii)}\ \ e^+e^- \to Z \to PS_i \to \bar{f}fS_i\\
&\text{(iv)}\ \ e^+e^- \to \gamma \to \bar{f}f \to \bar{f}fS_i.
\end{aligned} \tag{13}$$

At higher center of mass energies $\sqrt{s} \geq 500$ GeV the channels with virtual photon exchange become comparable to those with $Z_0^*$ exchange, but are negligible at LEP energies.

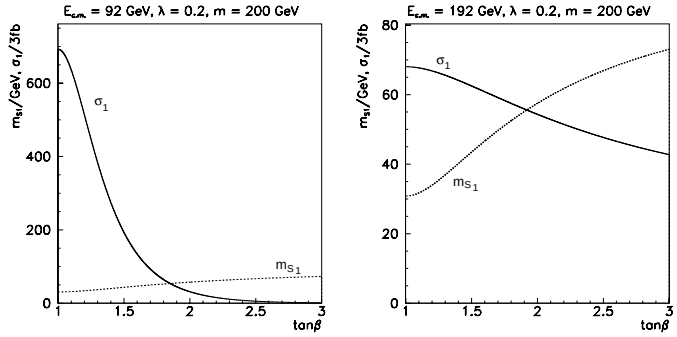


(a) (b)

**Fig. 5a,b.** $m_{S_1,\,\mathrm{tree}}$ (dashed line) and $\sigma_1$ (solid line) for $\lambda = 0.2$, $m = 200\,\mathrm{GeV}$: **a** $\sqrt{s} = 92\,\mathrm{GeV}$, **b** $\sqrt{s} = 192\,\mathrm{GeV}$

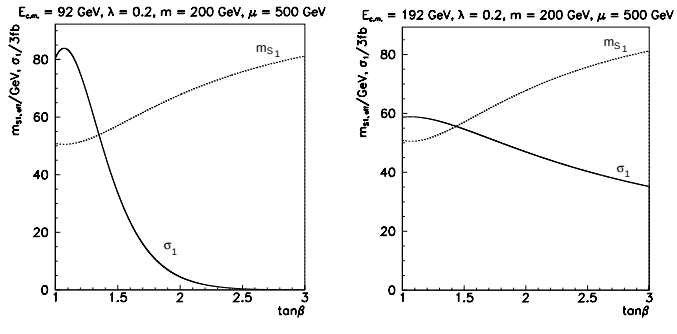


(a) (b)

**Fig. 6a,b.** $m_{S_1,\,\mathrm{eff}}$ (dashed line) and $\sigma_1$ (solid line) for $\lambda = 0.2$, $m = 200\,\mathrm{GeV}$, $\mu = 500\,\mathrm{GeV}$: **a** $\sqrt{s} = 92\,\mathrm{GeV}$, **b** $\sqrt{s} = 192\,\mathrm{GeV}$

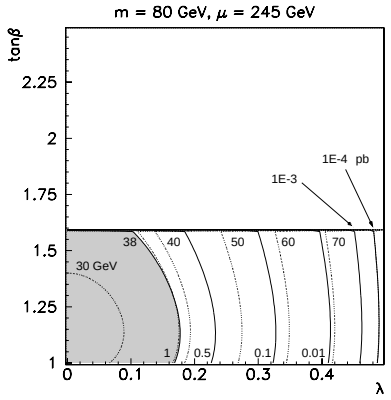


**Fig. 7.** $\sigma_1$ (solid line) and $m_{S_1}$ (dashed line) at one-loop level for $\sqrt{s} = 92\,\mathrm{GeV}$, $\mu = 245\,\mathrm{GeV}$ and m=80 GeV. The region of $\sigma_1 \geq 1$fb is shaded

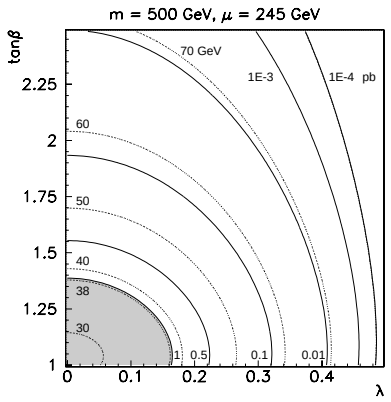


**Fig. 8.** $\sigma_1$ (solid line) and $m_{S_1}$ (dashed line) at one-loop level for $\sqrt{s} = 92\,\mathrm{GeV}$, $\mu = 245\,\mathrm{GeV}$ and m=500 GeV. The region of $\sigma_1 \geq 1$fb is shaded

In [10] we used $\tan\beta$, $m_{S_1}$ and $m_P$ as parameters. In the present case it is more convenient to take $\tan\beta$, $\lambda$ and $m$ as independent parameters.

In order to illustrate the effect of radiative corrections on the cross section $\sigma$, we plot $\sigma$ and $m_{S_1}$ as functions of $\tan\beta$ for $\lambda = 0.2$, $m = 200$ GeV at tree level in Fig. 5a(5b) and for $\lambda = 0.2$, $m = 200$ GeV, $\mu = 200$ GeV at one-loop level in Fig. 6a (6b) for $\sqrt{s} = 92$ GeV (192 GeV). These figures show that radiative contributions are rather large in the region of small $\tan\beta$, more significant for $\sqrt{s} = 92$ GeV than for $\sqrt{s} = 192$ GeV.

However it turns out that they do not significantly affect the region of $m_{S_1}$ which may be explored by the $e^+e^-$-colliders, as we will discuss in the following.

First we analyze the LEP1 data. The discovery limit is 1pb [14,13]. We scanned the parameter space by considering $m$ from 80 GeV to 1000 GeV and varying $\mu$ from 245 GeV to 1000 GeV. A systematic trend is that at a given point in the $\tan\beta$-$\lambda$-plane $\sigma_1$ decreases, whereas $m_{S_1}$ increases compared to their respective tree level values. This trend strongly depends on $\mu$, but only smoothly on $m$. Figs. 7-8 ($\mu = 245$ GeV) show that the line of $\sigma_1 = 1$ pb and the line of $m_{S_1} = 38$ GeV move with m, but the change of their relative position remains negligible small. The largest $m_{S_1}$ line which is entirely inside the region of $\sigma_1 \geq 1$ pb is slightly higher than 38 GeV, whereas at the tree level case it is slightly lower than 38 GeV. The difference is smaller than 1 GeV.

For increasing $\mu$ the change of $m_{S_1}$ and $\sigma_1$ compared to their tree level values gets more pronounced as shown in Fig. 9. Nevertheless the analysis shows that the relative position of the contour lines for $\sigma_1 = 1$pb and for $m_{S_1} = 38\,\mathrm{GeV}$ is not changed by varying $\mu$.

In summary we conclude that the LEP1 data, if interpreted in the frame of the one-loop effective potential of our model, yield almost the same experimental lower limit (less than 1 GeV difference) on $m_{S_1}$ as in the tree level case, namely about 38 GeV.

We did similar calculations for LEP2, LC-500, LC-1000, LC-2000 and fount the contributions of the radiative corrections in term of the one-loop effective potential to be less than 5%.

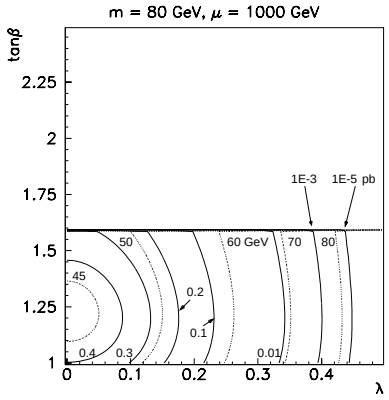


**Fig. 9.** $\sigma_1$ (solid line) and $m_{S_1}$ (dashed line) at one-loop level for $\sqrt{s} = 92\,\text{GeV}$, $\mu = 1000\,\text{GeV}$ and m=80 GeV. The region of $\sigma_1 \geq 1\text{fb}$ is shaded

**Table 1.** Couplings of neutral Higgs bosons relative to SM value

| $\Phi$ | $g_{\Phi u\bar{u}}$ | $g_{\Phi d\bar{d}}$ | $g_{\Phi VV}$ |
|---|---|---|---|
| $S_1$ | $\frac{\cos\alpha}{\sin\beta}$ | $-\frac{\sin\alpha}{\cos\beta}$ | $\sin(\beta-\alpha)$ |
| $S_2$ | $\frac{\sin\alpha}{\sin\beta}$ | $\frac{\cos\alpha}{\cos\beta}$ | $\cos(\beta-\alpha)$ |
| $P$ | $\cot\beta$ | $\tan\beta$ | 0 |

**Table 2.** Normalized couplings of two Higgs to one gauge boson

| $\Phi$ | $g_{W^\pm H^\pm \Phi}$ | $g_{ZP\Phi}$ |
|---|---|---|
| $S_1$ | $\mp\cos(\alpha-\beta)$ | $\cos(\alpha-\beta)$ |
| $S_2$ | $\mp\sin(\alpha-\beta)$ | $\sin(\alpha-\beta)$ |
| $P$ | 1 | 0 |

## 5 Higgs couplings and decays

We now turn to the investigation of decays of the Higgs bosons. The results obtained in this section are based mainly on tree level calculations. Besides the two-body decay channels we also included the most important three-body decays channels in the analysis. We only included three-body decays when they had significant branching ratios and the corresponding two-body decay was kinematically forbidden in the whole parameter space.

Before we come to the actual investigation of the decays we will discuss the couplings relevant for Higgs decays as some general features of the Higgs decay pattern may already be derived from the couplings.

### 5.1 Higgs couplings

The couplings of the neutral Higgs bosons $S_1$, $S_2$ and $P$ to fermion and gauge boson pairs are shown in Table 1 relative to the standard model values of

$$g_{\Phi_{SM} f\bar{f}} = \frac{g_2 m_f}{2m_W}$$
$$g_{\Phi_{SM} VV} = \frac{g_2 m_V^2}{m_W}. \tag{14}$$

The coupling of the charged Higgs boson $H^+$ to fermions is given by

$$g_{H^+ u\bar{d}} = \frac{g_2}{2\sqrt{2}m_W} \left[(m_d \tan\beta + m_u \cot\beta) + (m_d \tan\beta - m_u \cot\beta)\gamma_5\right]. \tag{15}$$

The couplings of two Higgs bosons to one gauge boson are listed in Table 2. They are given relative to the values

$$g_W = \frac{g_2}{2}(p+p')^\mu$$
$$g_Z = \frac{g_2}{2\cos\theta_W}(p+p')^\mu \tag{16}$$

where p (p') is the incoming (outgoing) momentum of the neutral (charged) Higgs boson.

Numerical results show that for $m \gtrsim 200\,\text{GeV}$ the mass of the lighter CP-even neutral Higgs boson $S_1$ approaches its maximum value for fixed $\tan\beta$ and $\lambda$ and the couplings of $S_1$ are approximately standard-model-like. In this region of parameter space $|\cos(\alpha-\beta)| \lesssim 0.1$ so that the coupling of $S_2$ to gauge boson pairs becomes relatively small and furthermore the fermionic couplings of $S_2$ approach that of the pseudoscalar Higgs boson $P$.

Finally the couplings $S_2S_1S_1$ and $S_2PP$ are relevant for Higgs decays. They are given by

$$g_{S_2S_1S_1} = \frac{g_2 m_Z}{2\cos\theta_W}\left[\cos 2\alpha\ \cos(\alpha+\beta) - 2\sin 2\alpha\ \sin(\alpha+\beta)\right] - \frac{4}{5}\frac{\lambda^2 m_W}{g_2}\left[2\cos 2\alpha\ \cos(\alpha+\beta) - \sin 2\alpha\ \sin(\alpha+\beta)\right] \tag{17}$$

and

$$g_{S_2PP} = \frac{g_2 m_Z}{2\cos\theta_W}\cos 2\beta\ \cos(\alpha+\beta) - \frac{4}{5}\frac{\lambda^2 m_W}{g_2}\left[\cos(\alpha+\beta) + \cos 2\beta\ \cos(\alpha+\beta)\right]. \tag{18}$$

The couplings given in Tables 1 and 2 have the same form as those in the MSSM [15]. The difference lies in the mixing angle $\alpha$ which is given by a different expression in our model. It is now possible for $\alpha$ to take such values that some of the expressions in Table 1 and 2 and therefore the corresponding couplings vanish.

The conditions for this decouplings are displayed in Table 3 together with the corresponding conditions in the MSSM. As opposed to the MSSM the decoupling is also possible for $\tan\beta \neq 1$ in the nonlinear SU(5) model and not only $\cos(\alpha-\beta)$ but also $\sin\alpha$ can vanish for $\tan\beta \neq 1$.

When $\sin\alpha = 0$ the light neutral Higgs boson $S_1$ will decouple from down-type fermions while the heavy neutral Higgs boson $S_2$ decouples from up-type fermions as can be

**Table 3.** conditions for vanishing of the relative couplings in the nonlinear SUSY SU(5) model and the MSSM

| Condition | nonlin. SUSY SU(5) | MSSM |
|---|---|---|
| $\sin\alpha = 0 \Leftrightarrow$ | $\tan\beta \neq 1 \wedge \frac{2}{5}\lambda^2 v^2 = m_Z^2 + \mu^2$ | impossible |
| $\cos\alpha = 0 \Leftrightarrow$ | impossible | impossible |
| $\sin(\alpha-\beta) = 0 \Leftrightarrow$ | $\tan\beta = 1 \wedge \frac{2}{5}\lambda^2 v^2 > m_Z^2 + \mu^2$ | impossible |
| $\cos(\alpha-\beta) = 0 \Leftrightarrow$ | $(\tan\beta = 1 \wedge \frac{2}{5}\lambda^2 v^2 < m_Z^2 + \mu^2)$ | $\tan\beta = 1$ |
| | $\vee(\tan\beta \neq 1 \wedge \frac{2}{5}\lambda^2 v^2 = m_Z^2)$ | |

seen from Table 1. If $\cos(\alpha-\beta) = 0$ the heavy Higgs boson $S_2$ decouples from gauge boson pairs, and the couplings of $S_1$ to one Higgs and one gauge boson vanish. Furthermore $\cos(\alpha-\beta) = 0$ implies $g_{S_2 S_1 S_1} = 0$.

These decouplings have great phenomenological relevance due to a number of reasons. The first is that the decay $S_1 \to b\bar{b}$ is the dominant decay mode for sufficiently light Higgs bosons in nearly all models and therefore the searches of Higgs bosons in experiments concentrates on this mode. The second reason concerns the production mechanisms for the heavy neutral Higgs boson $S_2$. Among the most important processes are the Higgs-Strahlung process for the production at $e^+e^-$-machines and the $W^+W^-$-fusion mechanism for the production at hadron colliders [16]. If $S_2$ decouples from gauge boson pairs, these production mechanisms are no longer available and the production and detection of the heavy neutral CP-even Higgs boson $S_2$ may be quite difficult.

## 5.2 Higgs decays

### 5.2.1 $S_1$

The decay width of the neutral Higgs bosons in fermion pairs is given by

$$\Gamma(\Phi \to f\bar{f}) = \frac{N_c g_2^2}{32\pi} g_{\Phi f\bar{f}}^2 \frac{m_f^2}{m_W^2} m_\Phi \left(1 - 4\frac{m_f^2}{m_\Phi^2}\right)^p, \quad (19)$$

with $p = \frac{3}{2}(\frac{1}{2})$ for $\Phi = S_1, S_2(P)$ and the relative couplings from Table 1.

In the region where $m_{S_1}$ is near its upper bound decays into one real and one virtual gauge boson become important. If one assumes the fermions produced in the decay of the virtual gauge boson to be massless and sums over all possible fermions in the final state one gets the decay width for this channel

$$\Gamma(S_1 \to VX) = \int_{2\sqrt{\mu_V}}^{1+\mu_V} dx \frac{g_2^4}{512\pi^3} f_V m_{S_1} \frac{\sqrt{x^2 - 4\mu_V}}{(1-x)^2 + \mu_V\gamma_V} \cdot \left[x^2 + 8\mu_V - 12\mu_V x + 12\mu_V^2\right] \quad (20)$$

with

$$f_W = 3$$

$$f_Z = \frac{1}{4\cos\theta_W^4}\left[7 - \frac{40}{3}\sin^2\theta_W + \frac{160}{9}\sin^4\theta_W\right] \quad (21)$$

and $\mu_V = \frac{m_V^2}{m_{S_1}^2}$, $\gamma_V = \frac{\Gamma_V^2}{m_{S_1}^2}$ being the scaled mass and width of the gauge boson $V$.

### 5.2.2 $S_2$

While $S_1$ may not decay into real gauge boson pairs this decay channel is open for $S_2$ over a wide range of parameters. The decay width for this channel is

$$\Gamma(S_2 \to VV) = \frac{g_2^2 f}{128\pi}\cos^2(\alpha-\beta)\sqrt{1-x_V}\frac{m_{S_2}^3}{m_W^2} \cdot \left[1 - x_V + \frac{3}{4}x_V^2\right] \quad (22)$$

with $f = 1(2)$ for $V = Z(W)$ and $x_V = 4\frac{m_V^2}{m_{S_2}^2}$.

When kinematically allowed decays into pairs of neutral Higgs bosons may also become important, the relevant decay width is

$$\Gamma(S_2 \to \Phi\Phi) = \frac{g_{S_2\Phi\Phi}^2}{32\pi}\frac{1}{m_{S_2}}\sqrt{1 - 4\frac{m_\Phi^2}{m_{S_2}^2}}, \quad (23)$$

with $\Phi = S_1(P)$ and the couplings from (17) and (18).

The decay $S_2 \to ZP$ is kinematically impossible, but in parts of the parameter space the decay $S_2 \to Z^*P \to f\bar{f}P$ is important. The decay width for this channel is given by

$$\Gamma(S_2 \to Z^*P \to XP) = \int_{2\sqrt{\mu_P}}^{1+\mu_P} dx \frac{g_2^2 g_{ZPS_2}^2}{192\pi^3\cos^2\theta_W} m_{S_2} \cdot \left(\frac{21}{8} - 5\sin^2\theta_W + \frac{20}{3}\sin^4\theta_W\right) \cdot \frac{\left(x^2 - 4\mu_P\right)^{\frac{3}{2}}}{(1 + \mu_P - \mu_Z - x)^2 + \mu_Z\gamma_Z}, \quad (24)$$

with $\mu_P = \frac{m_P^2}{m_{S_2}^2}$, $\mu_Z = \frac{m_Z^2}{m_{S_2}^2}$ and $\gamma_Z = \frac{\Gamma_Z^2}{m_{S_2}^2}$.

### 5.2.3 $P$

The pseudoscalar Higgs boson $P$ dominantly decays into fermion pairs with the decay width given by (19). Since it does not couple to gauge boson pairs the only remaining relevant decay mode is the decay into $S_1 Z$ which is sizable in parts of the parameter space. The decay width for this channel is given by

$$\Gamma(P \to ZS_1) = \frac{g_2^2}{64\pi\cos^2\theta_W}\cos^2(\beta-\alpha)\frac{1}{m_P^3}\lambda^{\frac{1}{2}}(m_P^2, m_Z^2, m_{S_1}^2) \cdot \left[m_Z^2 - 2(m_P^2 + m_{S_1}^2) + \frac{1}{m_Z^2}(m_P^2 - m_{S_1}^2)^2\right], \quad (25)$$

where

$$\lambda(a,b,c) = a^2 + b^2 + c^2 - 2(ab + ac + bc). \tag{26}$$

#### 5.2.4 $H^+$

In the case of the charged Higgs boson $H^+$ the width for the decay into two fermions reads

$$\begin{aligned}\Gamma(H^+ \to u\bar{d}) = {} & \frac{3g_2^2}{32\pi}\frac{1}{m_W^2 m_{H^\pm}^3}\lambda^{\frac{1}{2}}(m_{H^\pm}^2, m_u^2, m_d^2) \\ & \cdot \left[(m_d^2 \tan^2\beta + m_u^2 \cot^2\beta)\right. \\ & \left.\cdot (m_{H^\pm}^2 - m_u^2 - m_d^2) - 4m_u^2 m_d^2\right]. \end{aligned} \tag{27}$$

If kinematically allowed the decay $H^+ \to t\bar{b}$ is dominant, but even well below the $t\bar{b}$-threshold the decay $H^+ \to t^*\bar{b}$ in a virtual top-quark and a real b-quark has significant branching ratio. The decay width for this three-body decay is given by

$$\begin{aligned}&\Gamma(H^+ \to W^+ b\bar{b}) = \\ &\int_0^{1-\mu_W} dx\, \frac{N_c g_2^4 \cot^2\beta}{2048\pi^3}\frac{m_t^4}{m_W^4} m_{H^\pm}\frac{1}{(1-\mu_t - x)^2 + \mu_t\gamma_t} \\ &\cdot\frac{(1-\mu_W - x)x}{(1-x)^2}\left[(1-x)^2 + \mu_W(1-x) - 2\mu_W^2\right], \end{aligned} \tag{28}$$

with $\mu_t = \frac{m_t^2}{m_{H^+}^2}$, $\gamma_t = \frac{\Gamma_t^2}{m_{H^+}^2}$, $\mu_W = \frac{m_W^2}{m_{H^+}^2}$ and $\gamma_W = \frac{\Gamma_W^2}{m_{H^+}^2}$.

Besides the fermionic decay channels, decays into one Higgs and one gauge boson are important. Of these only the decay $H^+ \to W^+ S_1$ is allowed by kinematics, the decay width being

$$\begin{aligned}&\Gamma(H^+ \to W^+ S_1) = \\ &\frac{g_2^2}{64\pi}\cos^2(\beta-\alpha)\frac{1}{m_{H^+}^3}\lambda^{\frac{1}{2}}(m_{H^\pm}^2, m_W^2, m_{S_1}^2) \\ &\cdot\left[m_W^2 - 2(m_{H^\pm}^2 + m_{S_1}^2) + \frac{1}{m_W^2}(m_{H^\pm}^2 - m_{S_1}^2)^2\right]. \end{aligned} \tag{29}$$

While the decays $H^+ \to W^+ S_2$ and $H^+ \to W^+ P$ are kinematically not allowed the corresponding processes with a virtual $W^+$ boson become relevant in parts of the parameter space. The decay widths for these channels are given by

$$\begin{aligned}\Gamma(H^+ \to W^{+*}\Phi \to X\Phi) = {} & \int_{2\sqrt{\mu_\Phi}}^{1+\mu_\Phi} dx\, \frac{9g_2^4 g_{W^\pm H^\pm \Phi}^2}{256\pi^3} m_{H^+} \\ & \cdot\frac{\left(x^2 - 4\mu_\Phi\right)^{\frac{3}{2}}}{(1+\mu_\Phi - \mu_W - x)^2 + \mu_W\gamma_W}, \end{aligned} \tag{30}$$

where $\mu_\Phi = \frac{m_\Phi^2}{m_{H^+}^2}$ for $\Phi = S_2$ or $P$ and the normalized couplings $g_{W^\pm H^\pm \Phi}$ from Table 2.

#### 5.2.5 Discussion of results

We now come to the discussion of the decay pattern of the Higgs bosons. In general the Higgs bosons will dominantly decay into the heaviest particles allowed by kinematics. Three body decays involving virtual gauge bosons will normally not have branching ratios above a few percent unless close to the threshold for production of real gauge bosons. This general pattern is well known from the MSSM [17] but in our model there are further complications due to the above mentioned decouplings in the Higgs sector. We will first neglect these decouplings in our discussion of the decay pattern and then investigate the effects of the decouplings on the decay pattern separately.

As in the MSSM the decay pattern of the lightest neutral Higgs boson $S_1$ is quite simple. It dominantly decays into b-quark pairs with decays into c's and $\tau$'s contributing about 5-10% each (Fig. 11). Only for values of $\lambda$ above 0.7 three-body decays into gauge bosons may have branching ratios in the percent range (Fig. 15).

As already discussed the couplings of $S_1$ are standard-model-like in the region $m \gtrsim 200\,\mathrm{GeV}$ and the fermionic couplings of $S_2$ approach those of $P$, therefore depending nearly exclusively on $\tan\beta$. Because the masses of the heavy Higgs bosons $S_2$,$P$ and $H^\pm$ nearly exclusively depend on $m$ in this region, the decay pattern of these particles is approximately independent of $\lambda$. Of course this does not take into account the decoupling effects in the Higgs gauge boson couplings, but since these couplings only depend on $\lambda$ they can be investigated separately. Furthermore the Higgs couplings to gauge bosons are suppressed by $\cos(\alpha-\beta)$ and therefore decays to gauge bosons are not among the dominant decay modes.

The dependence of the decay widths and branching ratios on the parameter $m$ and therefore on the Higgs boson masses can be seen from Figs. 10 and 11 which nearly reproduce the decay pattern of the MSSM. It can be seen from these figures that decays containing a $S_2$ or $P$ in the final state are not relevant for values of $m \gtrsim 100\,\mathrm{GeV}$. These are the decays $S_2 \to PP$, $S_2 \to ZP$, $H^+ \to W^+ S_2$ and $H^+ \to W^+ P$. In fact the only region of the parameter space where these modes become relevant is for very small values of $m$ and $\tan\beta$ near 1 (Fig. 14).

The case of large $\tan\beta$ is not shown, but as in the MSSM decays into $t\bar{t}$ lose significance while the $b\bar{b}$ decay channel will eventually become the dominant one for sufficiently high $\tan\beta$. One has to note though that a large value of $\tan\beta$ implies a large $m$ in our model.

We now come to the discussion of the decouplings in the Higgs sector. The decoupling from gauge bosons, which happens for a fixed value of $\lambda \sim 0.59$ given by $\frac{2}{5}\lambda^2 v^2 = m_Z^2$ is illustrated in Fig. 15. The value of $m$ is chosen so that decays into top quark pairs are not possible. The impact of the decoupling on the absolute decay width is negligible except for $S_2$, where not only the decays into gauge bosons but also decays into the light Higgs boson $S_1$ are affected by the decoupling.

The decoupling involving fermions which happens for $\sin\alpha = 0$ is illustrated in Fig. 14. The most significant change of the decay pattern happens in the case of the

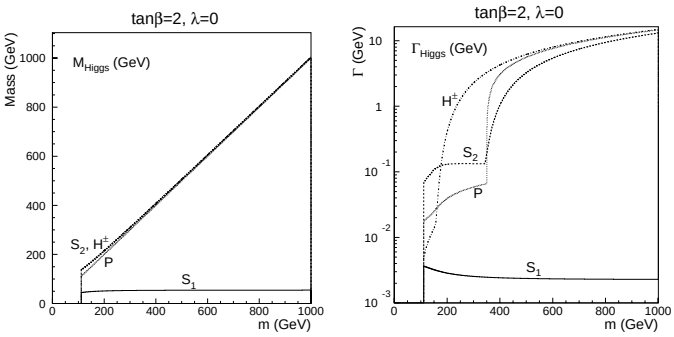


(a) (b)

**Fig. 10a,b.** Masses and total decay widths of Higgs bosons for $\lambda = 0$ and $\tan\beta = 2$

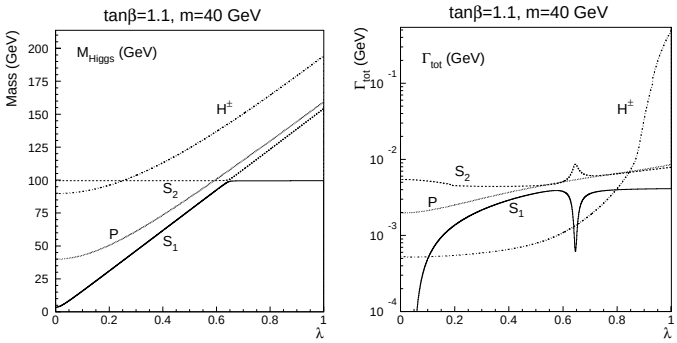


(a) (b)

**Fig. 12a,b.** Masses and total decay widths of Higgs bosons for $\tan\beta = 1.1$ and $m = 40\,\mathrm{GeV}$

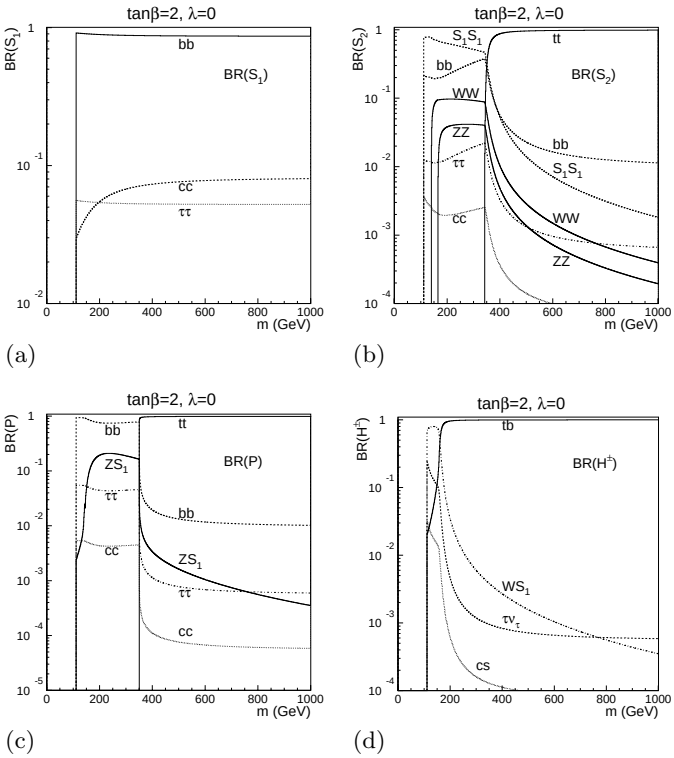


(a) (b) (c) (d)

**Fig. 11a–d.** Branching ratios of Higgs bosons for $\lambda = 0$ and $\tan\beta = 2$

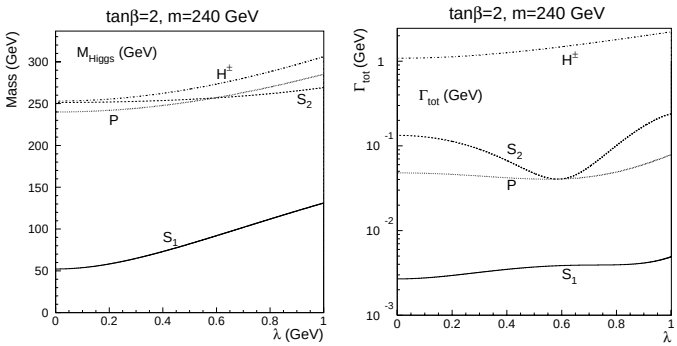


(a) (b)

**Fig. 13a,b.** Masses and total decay widths of Higgs bosons for $\tan\beta = 2$ and $m = 240\,\mathrm{GeV}$

light neutral Higgs boson $S_1$, where the dominant decay mode $S_1 \to b\bar{b}$ vanishes due to the decoupling. Instead this mode is replaced by the $c\bar{c}$ channel. It is therefore important for experimental searches not only to search for Higgs bosons in the $b\bar{b}$ but also in the $c\bar{c}$ decay channel.

### 5.2.6 Radiative corrections to $\Gamma(S_2 \to S_1 S_1)$

Although we have shown that the characteristic decouplings of Higgs bosons in this model are phenomenologically important, our analyzes so far only considered the tree-level couplings. But even if the tree-level couplings vanish, radiative corrections may become important and should be taken into account.

In order to estimate the effect of the radiative corrections on the decoupling we investigated the process $S_2 \to S_1 S_1$. Because only scalar particles are involved this is the simplest process affected by the decouplings. Furthermore we are only interested in a qualitative discussion of the effects of the one-loop corrections and therefore we did not perform a complete one-loop calculation. Instead we only took the $S_2 S_1 S_1$-vertex into account, and here we restricted us to top- and bottom-quarks in the loop. However we did not take into account radiative corrections to particle masses, or any other parameters of the theory. Comparison of our results in the case of $\lambda = 0$ with a complete one-loop calculation for the decay width $\Gamma(S_2 \to S_1 S_1)$ in the MSSM [19] shows that our approach gives the right qualitative behavior.

The fermion-loop contribution to the $S_2 S_1 S_1$-coupling is given by

$$i\Gamma^{(1)}_{S_2 S_1 S_1} = (-1)\mu^{4-D} \int \frac{d^D k}{(2\pi)^D} \mathrm{Tr}\left[\frac{i(\not{k} + m_f)}{k^2 - m_f^2} i g_{S_2 f f}\right.$$

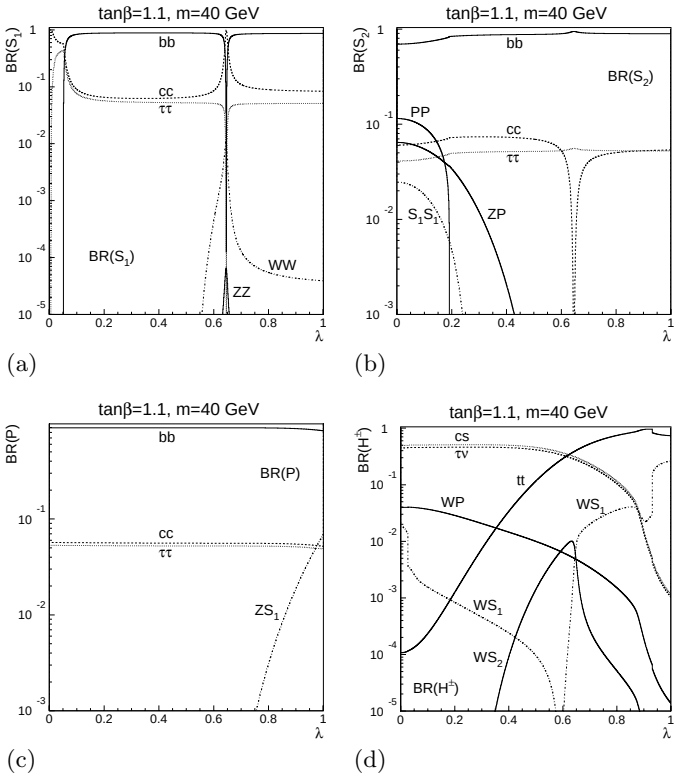


**Fig. 14a–d.** Branching ratios of Higgs bosons for $\tan\beta = 1.1$ and $m = 40\,\mathrm{GeV}$

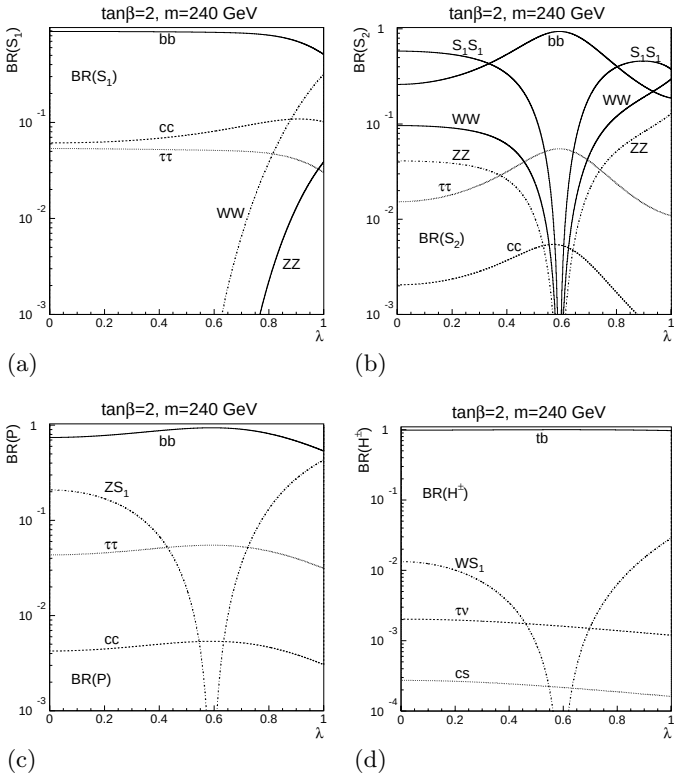


**Fig. 15a–d.** Branching ratios of Higgs bosons for $\tan\beta = 2$ and $m = 240\,\mathrm{GeV}$

$$\cdot\frac{i(\not k - \not p + m_f)}{(k-p)^2 - m_f^2} ig_{S_1ff} \frac{i(\not k - \not q + m_f)}{(k-q)^2 - m_f^2} ig_{S_1ff}\Bigg], \qquad (31)$$

with the naming conventions for the momenta as shown in Fig. 16.

If one performs the D-dimensional integration and sets all external momenta on-shell, the result for the fermion-loop contribution reads

$$\begin{aligned} i\Gamma^{(1)}_{S_2S_1S_1}\Big|_{\text{on-shell}} = \frac{i}{16\pi^2} g_{1ff}^2 g_{2ff} \big[4m_f(B_0(m_{S_2}^2, m_f, m_f) \\ +2B_0(m_{S_1}^2, m_f, m_f)) + (16m_f^3 - 2m_f[m_{S_2}^2 + 2m_{S_1}^2]) \\ C_0(m_{S_2}^2, m_{S_1}^2, m_{S_1}^2, m_f, m_f, m_f))\big], \end{aligned} \qquad (32)$$

where $B_0$ and $C_0$ are the scalar 2- and 3-point integrals introduced by t'Hooft and Veltman [18] which are defined by

$$\frac{i}{16\pi^2} B_0(q^2, m_1, m_2) = \qquad (33)$$
$$\mu^{4-D} \int \frac{d^Dk}{(2\pi)^D} \frac{1}{[k^2 - m_1^2][(k+q)^2 - m_2^2]}$$

$$\frac{i}{16\pi^2} C_0(p_1^2, (p_2-p_1)^2, p_2^2, m_1, m_2, m_3) = \qquad (34)$$
$$\mu^{4-D} \int \frac{d^Dk}{(2\pi)^D} \frac{1}{[k^2 - m_1^2][(k+p_1)^2 - m_2^2]} \qquad (35)$$
$$\cdot\frac{1}{[(k+p_2)^2 - m_3^2]} \qquad (36)$$

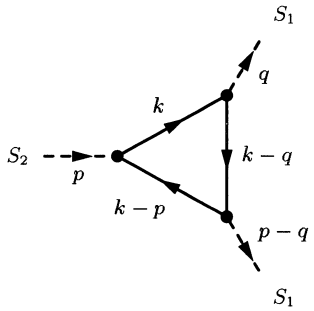


**Fig. 16.** One-loop contribution to $S_2S_1S_1$-vertex (arrows on scalar lines indicate direction of momentum)

The full one-loop corrected on-shell $S_2S_1S_1$-vertex is then given by

$$i\Gamma_{S_2S_1S_1}|_{\text{on-shell}} = ig_{S_2S_1S_1} + 2i\Gamma^{(1)}_{S_2S_1S_1}\Big|_{\text{on-shell}}. \qquad (37)$$

In Fig. 18 the results for the decay width $\Gamma(S_2 \to S_1S_1)$ are shown in the $\tan\beta$-$\lambda$-plane for $m = 400\,\mathrm{GeV}$ and Fig. 17 shows the dependence of the decay width on $\lambda$ alone for a constant value $\tan\beta = 2$. While the position of the zero in the decay width is independent of $\tan\beta$ in the tree level result this is not the case anymore with the radiatively corrected result. Instead the position of the zero gets shifted to smaller values of $\lambda$ and eventually reaches $\lambda = 0$ for $\tan\beta \sim 1.4$. This is the same behavior

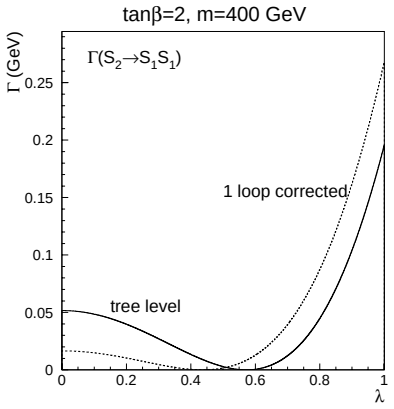


**Fig. 17.** Tree-level and 1-loop corrected decay width $\Gamma(S_2 \to S_1 S_1)$ for $\tan\beta = 2$ and $m = 400\,\mathrm{GeV}$

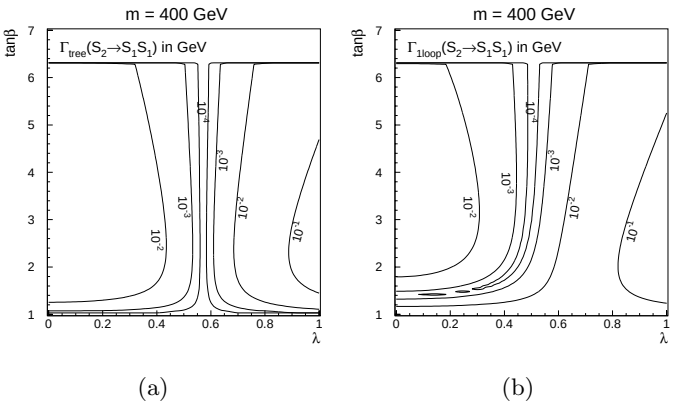


**Fig. 18.** Tree-level and 1-loop corrected decay width $\Gamma(S_2 \to S_1 S_1)$ for $m = 400\,\mathrm{GeV}$

as in the MSSM where radiative corrections can also lead to a vanishing decay width of this channel [19]. Therefore even when radiative corrections are taken into account there still is a decoupling in the $S_2 S_1 S_1$-coupling though at other values of the parameters.

## 6 Conclusion

Using the one-loop effective potential we have estimated radiative corrections to the tree level Higgs boson masses we determined in a previous paper [10]. As expected the correction is significant and it may become as much as 50 GeV. In contrast to the masses the radiative corrections to the experimental lower limits of $m_{S_1}$ on tree level [10] for LEP1,2 and future $e^+e^-$-colliders are not significant, smaller than 5%.

Finally we have investigated the decays of the Higgs bosons in our model. The general pattern is similar to that of the MSSM. So we have emphasized those aspects of our model which differ from MSSM. One such aspect is a certain decoupling phenomenon. We have showed in the case of $S_2 \to S_1 S_1$ that the decoupling exists still at one-loop level.

## References

1. V.P. Akulov and D.V. Volkov: Phys. Lett. B46 (1973) 109
2. O. Nachtmann, M. Wirbel: Z. Phys. C23 (1984) 85; Z. Phys. C23 (1984) 199; J.P. Ma, O. Nachtmann, M. Wirbel: Z. Phys. C30 (1986) 407; O. Nachtmann, T. Schucker: Z. Phys. C39 (1986) 291
3. S. Samuel, J. Wess: Nucl. Phys. B221 (1983) 153; Nucl. Phys. B226 (1983) 289; Nucl. Phys. B233 (1984) 488
4. S. Deser, B. Zumino, Phys. Rev. Lett. 38 (1977) 1433; D.Z. Freedman, A. Das, Nucl. Phys. B120 (1977) 221
5. B.R. Kim: Z. Phys. C67 (1995) 337
6. J. Ellis, J.F. Gunion, H.E. Haber, L. Roszkowski, F. Zwirner: Phys. Rev. D39 (1989) 844
7. S.W. Ham, H. Genten, B.R. Kim, S.K. Oh: Phys. Lett. B383 (1996) 178
8. H. Genten, S.W. Ham, B.R. Kim, S.K. Oh: Z. Phys. C76 (1997) 117
9. P. John, B.R. Kim: Z. Phys. C73 (1996) 169
10. H. Franz, B.R. Kim, M. Weber: Eur. Phys. J. C1 (1998) 649
11. S. Coleman, E. Weinberg: Phys. Rev. D7(1973)1888
12. B.R. Kim, S.K. Oh, PITHA 94/46
13. B.R. Kim, S.K. Oh, A. Stephan; *Proceedings of the Workshop on Physics and Experiments with Linear* $e^+e^-$ *Colliders, Hawaii 26.-30. April 1993* (1993) 860
14. J. Kalinowski: *Puzzles on the electroweak scale : Proceedings Z Ajduk et al* World Sci., Singapore, 1992 (317-323)
15. J.F. Gunion, H.E. Haber: Nucl. Phys. B272 (1986) 1
16. A. Djouadi: Int. J. Mod. Phys. A10 (1995) 1
17. A. Djouadi, J. Kalinowski, P.M. Zerwas: Z. Phys. C70 (1996) 435
18. G. t'Hooft, M. Veltman: Nucl. Phys. B153 (1979) 365
19. V. Barger, M.S. Berger, A.L. Stange, R.J.N. Phillips: Phys. Rev. D45 (1992) 4128; A. Brignole, F. Zwirner: Phys. Lett. B299 (1993) 72